The far C-terminus of MCAK regulates its conformation and spindle pole focusing

Hailing Zong[a], Stephanie K. Carnes[a], Christina Moe[a], Claire E. Walczak[b,*], and Stephanie C. Ems-McClung[b,*]
[a]Department of Biology and [b]Medical Sciences Program, Indiana University, Bloomington, IN 47405

ABSTRACT **To ensure proper spindle assembly, microtubule (MT) dynamics needs to be spatially regulated within the cell. The kinesin-13 MCAK is a potent MT depolymerase with a complex subcellular localization, yet how MCAK spatial regulation contributes to spindle assembly is not understood. Here we show that the far C-terminus of MCAK plays a critical role in regulating MCAK conformation, subspindle localization, and spindle assembly in *Xenopus* egg extracts. Alteration of MCAK conformation by the point mutation E715A/E716A in the far C-terminus increased MCAK targeting to the poles and reduced MT lifetimes, which induced spindles with unfocused poles. These effects were phenocopied by the Aurora A phosphomimetic mutation, S719E. Furthermore, addition of the kinesin-14 XCTK2 to spindle assembly reactions rescued the unfocused-pole phenotype. Collectively our work shows how the regional targeting of MCAK regulates MT dynamics, highlighting the idea that multiple phosphorylation pathways of MCAK cooperate to spatially control MT dynamics to maintain spindle architecture.**

Monitoring Editor
Stephen Doxsey
University of Massachusetts

Received: Oct 8, 2015
Revised: Feb 16, 2016
Accepted: Feb 25, 2016

INTRODUCTION

Eukaryotic cells rely on the microtubule (MT)-based mitotic spindle to faithfully segregate the replicated chromosomes during cell division. Assembly of the spindle is driven by the intrinsic dynamic instability of MTs, as well as by the MT-associated proteins that modulate both MT dynamics and organization (Walczak and Heald, 2008). To ensure proper spindle assembly, MT dynamics need to be spatially regulated within the cell. Despite the number of studies focused on the roles and regulation of MT dynamics modulators, the extent to which these modulators are spatially controlled in the spindle and the manner in which this spatial regulation contributes to spindle morphogenesis is not well understood.

Among the numerous MT dynamics modulators, the kinesin-13 mitotic centromere-associated kinesin (MCAK) is a potent MT depolymerase that has a complex subcellular localization (Wordeman and Mitchison, 1995; Walczak *et al.*, 1996; Desai *et al.*, 1999b). It is localized to the spindle poles, to the centromeres and kinetochores, in the cytoplasm, and to the plus tips of MTs (Wordeman and Mitchison, 1995; Moore *et al.*, 2005). The differential targeting of MCAK to functionally distinct parts of the spindle suggests that its localization should be dynamically regulated to control MT dynamics in different subspindle regions (Rizk *et al.*, 2009). Global depletion of MCAK disrupts spindle assembly in *Xenopus* extracts (Walczak *et al.*, 1996), whereas local inhibition of MCAK at centromeres and kinetochores causes defects in chromosome alignment and segregation without disrupting spindle assembly (Walczak *et al.*, 2002; Kline-Smith *et al.*, 2004). In addition, the tip-tracking population of MCAK is proposed to regulate MT density in interphase cells and ensure robust MT–kinetochore attachments by controlling MT length within the spindle (Domnitz *et al.*, 2012; Montenegro Gouveia *et al.*, 2010). However, the regulatory mechanisms that control the function of MCAK at the spindle poles are mostly unclear.

Structurally, MCAK contains an N-terminal domain (NT) that governs centromere targeting (Maney *et al.*, 1998; Walczak *et al.*, 2002), a class-specific neck domain that is required for MT depolymerization and enhances the on-rate to MTs (Maney *et al.*, 2001; Ovechkina *et al.*, 2002; Hertzer *et al.*, 2006; Cooper *et al.*, 2010), a central catalytic domain that binds MTs and hydrolyzes ATP, and a C-terminal

This article was published online ahead of print in MBoC in Press (http://www.molbiolcell.org/cgi/doi/10.1091/mbc.E15-10-0699) on March 3, 2016.

*Address correspondence to: Stephanie Ems-McClung (scems@indiana.edu), Claire Walczak (cwalczak@indiana.edu).

Abbreviations used: AMPPNP, adenylyl-imidodiphosphate; BSA, bovine serum albumin; CSF, cytostatic factor; CT, carboxy terminal domain; FCP, FRET control protein; FLIM, fluorescence lifetime imaging; FRET, Forster resonance energy transfer; GFP, green fluorescent protein; GMPCPP, guanylyl-(α, β)-methylene-diphosphonate; GST, glutathione *S*-transferase; mCer, mCerulean; mCit, mCitrine; MT, microtubule; NT, amino terminal domain.

domain (CT) that contributes to dimerization, catalytic activity, and spindle pole localization (Maney *et al.*, 2001; Hertzer *et al.*, 2006; Ems-McClung *et al.*, 2007). The catalytic domain together with the neck forms the minimal domain (MD) necessary to exert functional depolymerization activity in vitro (Maney *et al.*, 2001; Hunter *et al.*, 2003). Previous studies showed that the regulation of MCAK activity and its subcellular targeting are accomplished through a complex phosphoregulatory mechanism that acts on different domains of MCAK. In particular, Aurora B–dependent phosphorylation at S196 in the neck domain of MCAK inhibits MT depolymerization activity and promotes dissociation from the chromosome arms (Andrews *et al.*, 2004; Lan *et al.*, 2004; Ohi *et al.*, 2004; Zhang *et al.*, 2007). Aurora B phosphorylation of the NT positively influences MCAK targeting to centromeres, whereas Aurora A phosphorylation of S719 in the far CT of MCAK enhances spindle pole targeting in Ran-GTP spindles (Zhang *et al.*, 2007, 2008). Polo-like kinase 1 (Plk1) can also phosphorylate MCAK in the CT and control both protein stability and MT depolymerization activity (Zhang *et al.*, 2011). Recently Plk1-dependent phosphorylation at S715 (S719 in *Xenopus*) was proposed to regulate the MT depolymerase activity of MCAK at kinetochores to ensure faithful chromosome segregation (Shao *et al.*, 2015). Together these studies support the idea that different MCAK domains coordinately regulate its overall function and highlight how phosphorylation at distinct sites of MCAK contributes to the spatial control of MT dynamics.

Historically, the CT of MCAK has been implicated primarily in dimerization, which enhances MT depolymerization activity by increasing the ability of MCAK to remove tubulin subunits from the MT ends (Maney *et al.*, 2001; Hertzer *et al.*, 2006; Cooper *et al.*, 2010). Several lines of evidence support the idea that the CT not only plays structural roles in governing MCAK function but also coordinates with the NT/MD in controlling MCAK localization and activity. First, deletion of the last eight amino acids in the CT enhances lattice-induced ATPase activity (Moore and Wordeman, 2004), as well as abolishing the tip-tracking ability of MCAK, which requires binding to EB1 through the SKIP motif located in the NT (Moore *et al.*, 2005; Honnappa *et al.*, 2009). Second, the CT contributes to robust MT depolymerization activity and kinetochore targeting of MCAK (Hertzer *et al.*, 2006; Ems-McClung *et al.*, 2007). Third, MCAK conformation is maintained through a direct interaction between the CT and MD (Ems-McClung *et al.*, 2013). This conformation is regulated by Aurora B phosphorylation at S196, which switches MCAK conformation from "closed" to "open" and reduces MCAK affinity for MTs, hence inhibiting its MT depolymerase activity (Ems-McClung *et al.*, 2013). Finally, a recent study revealed the crystal structure of MD bound to a peptide corresponding to the last 25 amino acids of the CT and demonstrated that this far-CT region induces and stabilizes MD dimerization in solution (Talapatra *et al.*, 2015). Together these studies support the idea that the CT and MD coordinately control the conformation of MCAK. However, an important question remains as to how changes in MCAK conformation affect its physiological function in regulating MT dynamics during spindle assembly.

RESULTS

Residues E715 and E716 mediate the interaction of the CT with MD and are important for MCAK conformation

We previously demonstrated that the conformation *of Xenopus* MCAK is maintained through a direct interaction between the CT and MD (Ems-McClung *et al.*, 2013). To identify the minimal region of the CT that is required for this interaction, we made a series of glutathione *S*-transferase (GST)–CT deletion mutants and performed glutathione agarose pull-down experiments (Figure 1A). We found that GFP-tagged minimal domain (GMD) pulled down with GST-CT, whereas GMD did not pull down with GST-CTΔ27, GST-CTΔ62, or GST-CTΔ120 (Figure 1B and Supplemental Figure S1A). From these results, we conclude that the last 27 amino acids in the CT of MCAK are essential for the interaction between the CT and MD.

To narrow down the region necessary for this interaction, we made a shorter deletion that removed only the last 14 amino acids, CTΔ14 (Figure 1A). GST-CTΔ14 had slightly increased binding to GMD (Figure 1C and Supplemental Figure S1B), suggesting that the amino acids between Δ27 and Δ14 (703–716) are critical for the interaction between the CT and MD. Examination of this region reveals a pair of conserved glutamic acid residues, E715 and E716 (Supplemental Figure S1C). To abolish the negative charge, we mutated E715/E716 to alanine to create the 715AA mutant of the CT. Pull-down experiments showed that the binding of GMD to GST-CT(715AA) was inhibited relative to GST-CT and was similar to that of GST-Δ27 (Figure 1C and Supplemental Figure S1B). Taken together, these results demonstrate that residues E715 and E716 are critical for the binding of the CT to MD.

Having found that the binding of the CT to MD is disrupted by the 715AA mutation, we next asked whether disruption of this interaction also affects the conformation of MCAK. We performed Förster resonance energy transfer (FRET) assays with a biosensor of MCAK(715AA), which was constructed by fusing mCitrine (mCit) to the NT and mCerulean (mCer) to the CT of MCAK(715AA) (Ems-McClung *et al.*, 2013), referred to hereafter as FM(715AA). No FRET was detected from the addition of mCit and mCer individually, as indicated by a low mCit emission at 525 nm and a low FRET ratio of 0.38 ± 0.01 (FRET ratio = acceptor mCit emission at 525 nm divided by the donor mCer emission at 475 nm). High FRET was detected with the FRET control protein (FCP; fusion of mCit to mCer), as indicated by a high mCit emission at 525 nm and a high FRET ratio of 1.38 ± 0.04 (Figure 1D). Consistent with previous results, wild-type FMCAK displayed a high FRET ratio (1.34 ± 0.04; Figure 1E; Ems-McClung *et al.*, 2013). FM(715AA) displayed a 33% increase in the FRET ratio (1.83 ± 0.01) relative to FMCAK (Figure 1E). This suggests that the fluorophores are in closer proximity to each other, and indicates a more "closed" conformation of FM(715AA) relative to FMCAK in solution. To address whether this increased FRET of FM(715AA) was maintained when bound to the MT, we carried out fluorescence lifetime imaging microscopy (FLIM). The lifetime of FMCAK bound to MTs was 1.76 ns (95% confidence interval [CI] = 1.74–1.77 ns), which is significantly faster than 1.99 ns of the control MCAK-mCer bound to MTs (95% CI = 1.98–2.00 ns, $p < 0.0001$; Figure 1, F and G) and similar to our previously reported values (Ems-McClung *et al.*, 2013). FM(715AA) had an even faster lifetime of 1.62 ns (95% CI = 1.62–1.63 ns) relative to FMCAK ($p < 0.0001$), suggesting that FM(715AA) bound to the MTs in a more "closed" conformation. Together these results suggest that mutation of the far CT of MCAK disrupts the interaction of the CT with MD in a way that alters the overall conformation of MCAK and brings the fluorophores closer together, which we refer to as a more "closed" conformation.

MCAK(715AA) induces spindles with unfocused poles

To explore whether alteration of MCAK conformation by mutations in the far CT changes the function of MCAK in spindle assembly, we compared the ability of FMCAK or FM(715AA) to rescue spindle assembly in *Xenopus* egg extracts. Cycled extracts were mock depleted with immunoglobulin G (IgG; ΔIgG) or depleted of endogenous MCAK (ΔM) and then reconstituted with equal molar amounts

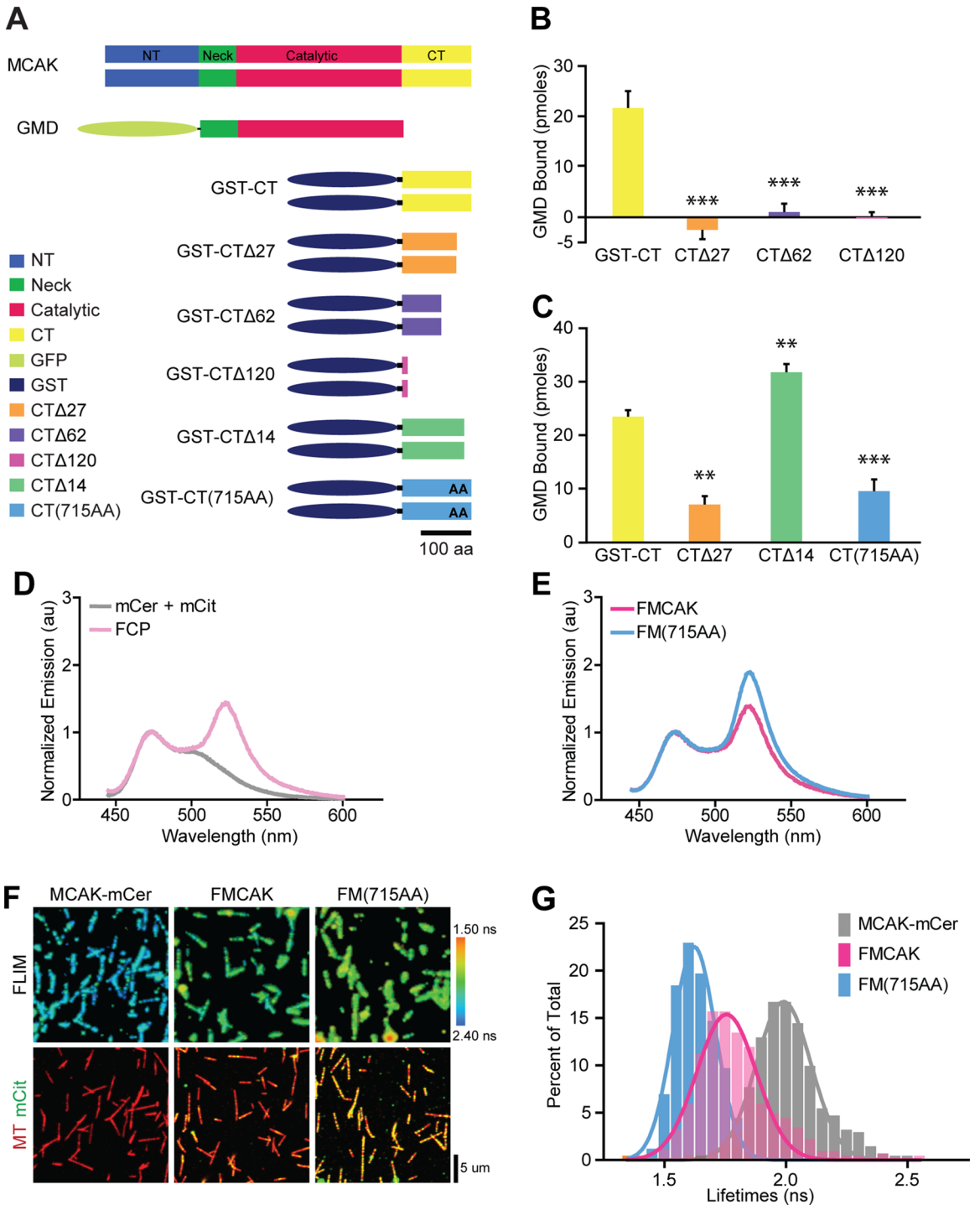

FIGURE 1: The far C-terminus of MCAK is important for MCAK conformation. (A) Schematic of MCAK, GMD, and the GST-CT deletion and point mutation proteins used in this study. (B, C) Quantification of bound GMD from glutathione agarose pull-down assays in which GST-CT or the indicated CT domain deletion or point mutant proteins were incubated with GMD. Graph represents mean ± SEM from six experiments. $^{**}p < 0.01$, $^{***}p < 0.001$. (D, E) Solution-based FRET assay was performed on control proteins (D) and the indicated FMCAK proteins (E) by exciting mCerulean at 433 nm and measuring the emission from 445 to 600 nm. Graphs represent mean of at least three experiments. (F) Representative FLIM images (top) and confocal images (bottom) of MCAK-mCer, FMCAK, or FM(715AA) bound to MTs. Lifetimes are represented by a heat map from red to blue, indicating lifetimes from 1.5 to 2.4 ns. Bar, 5 µm. (G) Frequency distribution of fluorescence lifetimes measured on MTs with the best-fit Gaussian curve from four separate experiments.

of FCP, FMCAK, or FM(715AA) before spindle assembly (Figure 2, A and B). MCAK-depleted extracts formed large MT asters with long MTs that were unable to form bipolar spindles, whereas mock-depleted extracts and MCAK-depleted extracts rescued with FMCAK formed normal bipolar spindles (Figure 2, C and D). Addition of FM(715AA) to MCAK-depleted extracts rescued spindle assembly

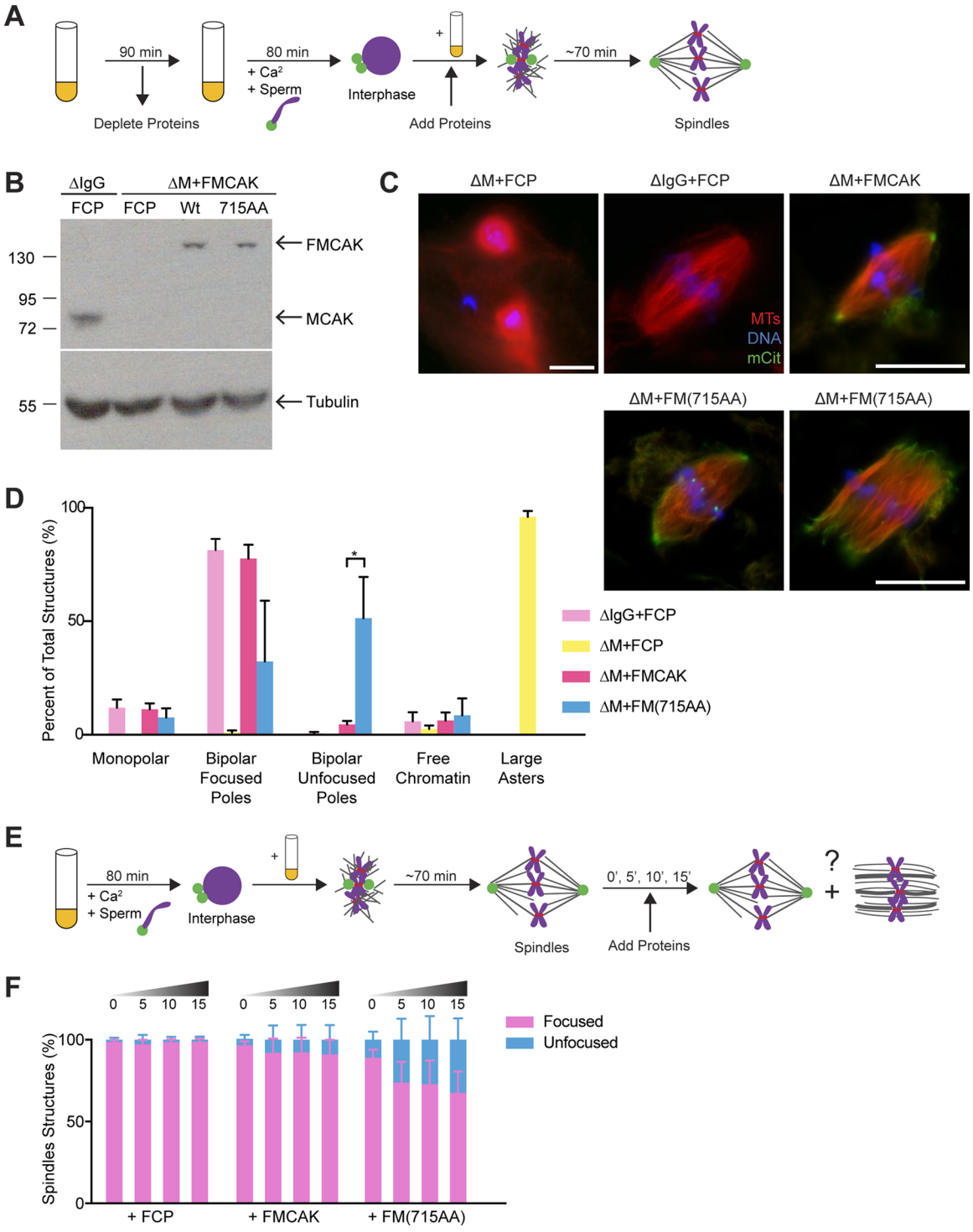

FIGURE 2: Mutations in the far C-terminus of MCAK induce spindles with unfocused poles. (A) *Xenopus* egg extracts were mock depleted or depleted with anti-MCAK antibodies and cycled into interphase. The extracts were reconstituted with 100 nM FCP, FMCAK, or FM(715AA) and cycled back into mitosis, and spindles were assembled. (B) Western blot of the depleted extracts reconstituted with the indicated proteins and probed with either anti-MCAK (top) or anti-tubulin (bottom). (C) Representative images from each depletion/add-back experiment. Note the different scale bar on ΔM+FCP. Scale bars, 20 μm. (D) Quantification of the percentage of total structures. Data represent mean ± SD ($n = 3$; 100 structures counted/per experiment). *$p < 0.05$. (E) Spindles were assembled in cycled *Xenopus* egg extracts for 60–70 min, and 100 nM FCP, FMCAK, or FM(715AA) was added to preformed spindles and incubated for 0, 5, 10, or 15 min. (F) Quantification of the percentage of total structures. Data represent mean ± SD ($n = 4$).

but caused a significant increase in the number of spindles with unfocused poles (Figure 2, C and D; 51 ± 18% for FM(715AA) vs. 5 ± 2% for FMCAK, $p < 0.05$). Similarly, addition of excess FM(715AA) to nondepleted cycled extracts also induced spindles with unfocused poles (34 ± 10% for FM(715AA) vs. 3 ± 3% for FMCAK, $p < 0.01$; Supplemental Figure S2). These results suggest that mutation of

E715/E716 disrupts aspects of spindle assembly that are important for MTs to be properly focused at the spindle poles.

To ask whether the unfocused poles could arise over time from spindles with initially focused poles, we analyzed the spindle structure in extracts with FCP, FMCAK, or FM(715AA) added after spindles were fully assembled. Proteins were incubated with preformed spindles for 0–15 min (Figure 2E). We found that the percentage of spindles with unfocused poles increased over time for FM(715AA) but not for FMCAK (Figure 2F), which indicates that FM(715AA) has a dominant effect on spindle pole focusing.

Mutation of E715 and E716 does not alter the MT depolymerization activity but increases the targeting of MCAK to spindle poles

The unfocused-pole phenotype generated by FM(715AA) suggested that this far-CT mutant has altered activity at the spindles poles compared with MCAK. We reasoned that there are two possibilities to explain this altered activity. One is that the enzymatic activity of FM(715AA) in depolymerizing MTs is changed. The other is that instead of a change in the inherent MT depolymerization activity for MCAK, the local concentration/localization of MCAK is changed at the spindle pole region, which results in a local increase in the MT depolymerization activity.

To test whether the MT depolymerization activity of FM(715AA) was altered, we performed a sedimentation-based MT depolymerization assay (Figure 3, A and B) and found no statistical difference in activity between FMCAK and FM(715AA), with EC_{50} values of 1.62 and 1.49 nM, respectively ($p = 0.57$; Figure 3B). This result shows that the E715A/E716A mutation in the far CT does not significantly influence the MT depolymerization activity of purified MCAK in vitro.

Given that the inherent MT depolymerization activity for FM(715AA) was not different from that for FMCAK, we speculated that a local increase in pole concentration of FM(715AA) could account for a local increase in the overall MT depolymerization activity that could cause unfocused spindle poles. To test this, we quantified the fluorescence intensity of FMCAK and FM(715AA) in the spindles formed in cycled extracts depleted of MCAK and reconstituted with each protein (Figure 3, C–E). The intensity ratio of added protein (indicated by mCit) to MT intensity (I_{mCit}/I_{MT}) was calculated and plotted versus its normalized position on the spindle (Figure 3D). For ΔIgG+FCP control, the intensity ratio of protein to MTs was low and flat across the spindle, with a slight increase around the poles. ΔM+FMCAK spindles had an increased protein fluorescence intensity ratio relative to ΔIgG+FCP, particularly at the poles, indicative of FMCAK localization to spindle MTs and enrichment at spindle poles. FM(715AA) on spindles with focused poles had an intensity ratio profile similar to FMCAK along the spindle body but an increased localization at the poles, which was statistically higher relative to FMCAK ($p < 0.05$; Figure 3E, top). In FM(715AA) spindles with unfocused poles, localization of FM(715AA) at the pole regions was even greater, and this increased localization extended toward the spindle equator ($p < 0.05$; Figure 3E, bottom). We conclude that the spindles with unfocused poles are caused by increased MCAK targeting to spindle poles rather than by a change in the biochemical MT depolymerization activity of MCAK.

715AA is sufficient to induce spindles with unfocused poles without centrosomes or kinetochores

In *Xenopus* extract spindles, MTs are nucleated from the spindle poles and around the chromatin and then sorted and focused at poles by the activity of molecular motors (Heald *et al.*, 1996; Walczak and Heald, 2008). Because FM(715AA) shows increased localization at the poles, we asked whether centrosomes are required for the unfocused-pole phenotype. We performed bead spindle assembly in extracts in which spindles can form around plasmid DNA–coated beads that lack both centrosomes and kinetochores (Heald *et al.*, 1996). Bead spindle assembly reactions were performed in parallel with cycled sperm spindle reactions in which excess FCP, FMCAK, or FM(715AA) was added (Figure 4A). Similar to FCP addition, FMCAK addition to sperm or bead spindles resulted in mostly bipolar spindles with focused poles (Figures 4, B and C, and Supplemental Figure S4). In contrast, addition of FM(715AA) caused an increase in the number of sperm spindles with unfocused poles (56 ± 19%), as well as a modest increase in the number of bead spindles with unfocused poles (20 ± 2%), which suggests that centrosomes contribute to some degree to this phenotype. In addition, we noticed that many of the bead spindles with unfocused poles were narrower than control bead spindles or sperm spindles with focused spindle poles, suggesting that disruption of pole focusing also causes defects in global spindle structure in the absence of kinetochores (Figure 4B). Taken together, our findings suggest that centrosomes and/or kinetochores contribute to the generation of the unfocused-pole phenotype, but that they are not absolutely required.

Enrichment of MCAK(715AA) at the poles inhibits antipolar MT growth and shortens MT lifetimes

Our findings so far suggest that the FM(715AA) mutant disrupts spindle poles through increased targeting that locally boosts MT depolymerization at the poles. It was shown that the metaphase spindles in *Xenopus* extracts are composed of a central barrel array composed of MTs growing from the chromatin and a polar array on each side composed of MTs emanating from the spindle poles (Yang *et al.*, 2008). To gain more insight into how the FM(715AA) mutant affected MT organization in the spindle, we imaged the plus tip–tracking protein EB1 and examined the distribution and direction of growing MTs in the spindle using plusTipTracker (Tirnauer *et al.*, 2004; Matov *et al.*, 2010; Applegate *et al.*, 2011). We observed that in both ΔM+FMCAK control spindles and ΔM+FM(715AA) focused spindles, there were similar numbers of EB1 comets throughout the spindle (707 ± 111 comets per ΔM+FMCAK spindle and 609 ± 68 comets per ΔM+FM(715AA) focused spindle; Figure 5, A and B, Supplemental Figure S5, A and B, and Supplemental Movie S1). In contrast, there were fewer EB1 comets in ΔM+FM(715AA) unfocused spindles (417 ± 62 comets/spindle), with a noticeable drop in the number of comets near the pole regions (Figure 5C, Supplemental Figure S5C, and Supplemental Movie S1). If we added excess FM(715AA) to preformed spindles, we occasionally observed spindles in the process of transitioning from a focused to an unfocused pole within 5 min after FM(715AA) addition (Supplemental Movie S2), consistent with our earlier fixed-time-point analysis (Figure 2F). We observed that in these spindles, the MT growth from the chromosomal region remained robust, whereas the amount of MTs emanating from the poles was greatly reduced.

To ascertain which MT array might be affected in ΔM+FM(715AA) unfocused spindles, we determined the distribution of comets across the spindle that were moving either toward the pole region (poleward), which likely emanate from the chromatin, or away from the pole region (antipolar), which likely originate from the poles (Figure 5, D–I). For ΔM+FMCAK spindles, the percentage of antipolar moving MTs was high around the pole region and lower at the midzone (Figure 5, D and G), indicating an enrichment of MT growth from the poles. Consistent with the existence of the two types of MT

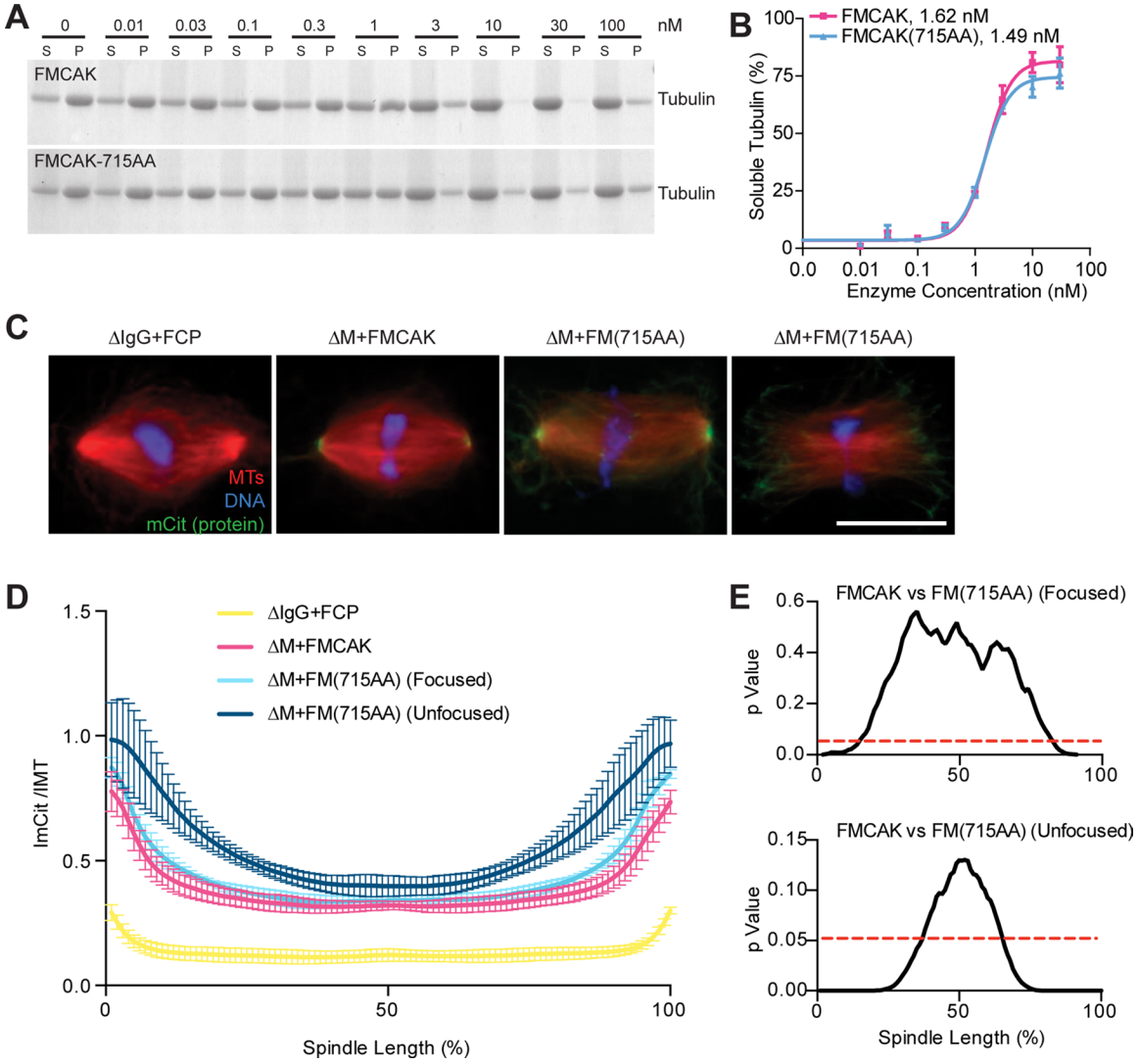

FIGURE 3: FM(715AA) shows no difference in MT depolymerization activity but has increased targeting to spindle poles. (A) The 715AA mutation does not significantly affect the ability of MCAK to depolymerize MTs in vitro. From 0 to 100 nM FMCAK or FM(715AA) was incubated with GMPCPP-stabilized MTs and then sedimented by centrifugation. Equivalent amounts of the soluble (S) and pellet (P) fractions were run on 10% SDS–PAGE gels, stained with Coomassie, and quantified by densitometry. (B) Quantification of EC_{50} from four independent experiments. Mean ± SEM for each enzyme concentration is graphed with the best-fit four-parameter nonlinear regression curve determined in Prism. (C) Representative images of spindles from MCAK-depleted and FCP, FMCAK, and FM(715AA) add-back reactions. Scale bar, 20 μm. (D) The ratio of the intensity of the localized protein (I_{mCit}) relative to the MT intensity (I_{MT}) calculated and plotted as a function of the normalized spindle length. Data represent mean ± SD from three separate extracts in which 10–20 spindle structures were analyzed per condition. (E) Student's *t* test analysis of the protein-to-MT intensity ratio (I_{mCit}/I_{MT}) across the spindle of FMCAK vs. FM(715AA). Red dashed line indicates $p = 0.05$.

arrays in the spindle, the percentage of antipolar-moving MTs at the pole regions (64 ± 7%) was significantly higher than at the midzone (40 ± 2%; $p < 0.0001$; Figure 5J). In ΔM+FM(715AA) spindles with focused poles, the population of antipolar EB1 comets was also greater at the pole region (59 ± 4%) than at the midzone (44 ± 5%; $p < 0.001$), and was similar to that of the ΔM+FMCAK control ($p = 0.17$ and 0.094, respectively; Figure 5, E, H, and J). However, in ΔM+FM(715AA) spindles with unfocused poles, the antipolar-growing MTs at the spindle poles (46 ± 10%) had a density similar to that of the midzone antipolar-growing MTs (43 ± 9%, $p = 0.66$), which was significantly less than those at the poles of ΔM+FMCAK spindles ($p < 0.01$) and ΔM+FM(715AA) focused spindles ($p < 0.05$; Figure 5, F, I, and J). These results are consistent with our hypothesis that the E715A/E716A mutant has increased targeting to the pole region, which subsequently disrupts the polar array, causing unfocused spindle poles.

Because MCAK is a potent catastrophe factor (Desai *et al.*, 1999b), increased localization of MCAK to the polar region could be expected to increase the MT catastrophe frequency at the poles, causing the EB1 tracks to dwell less and have shorter lifetimes. To assess the effects of ΔM+FM(715AA) on the behavior of the EB1 comets, we measured the lifetimes of all of the EB1 tracks at the pole and midzone regions (Figures 5K and Supplemental Figure S5, D–F). The lifetimes of EB1 comets were fitted to a single-exponential decay to determine the average lifetime (τ; Supplemental Figure S5, D–F). We found that the average lifetime of the EB1 comets in

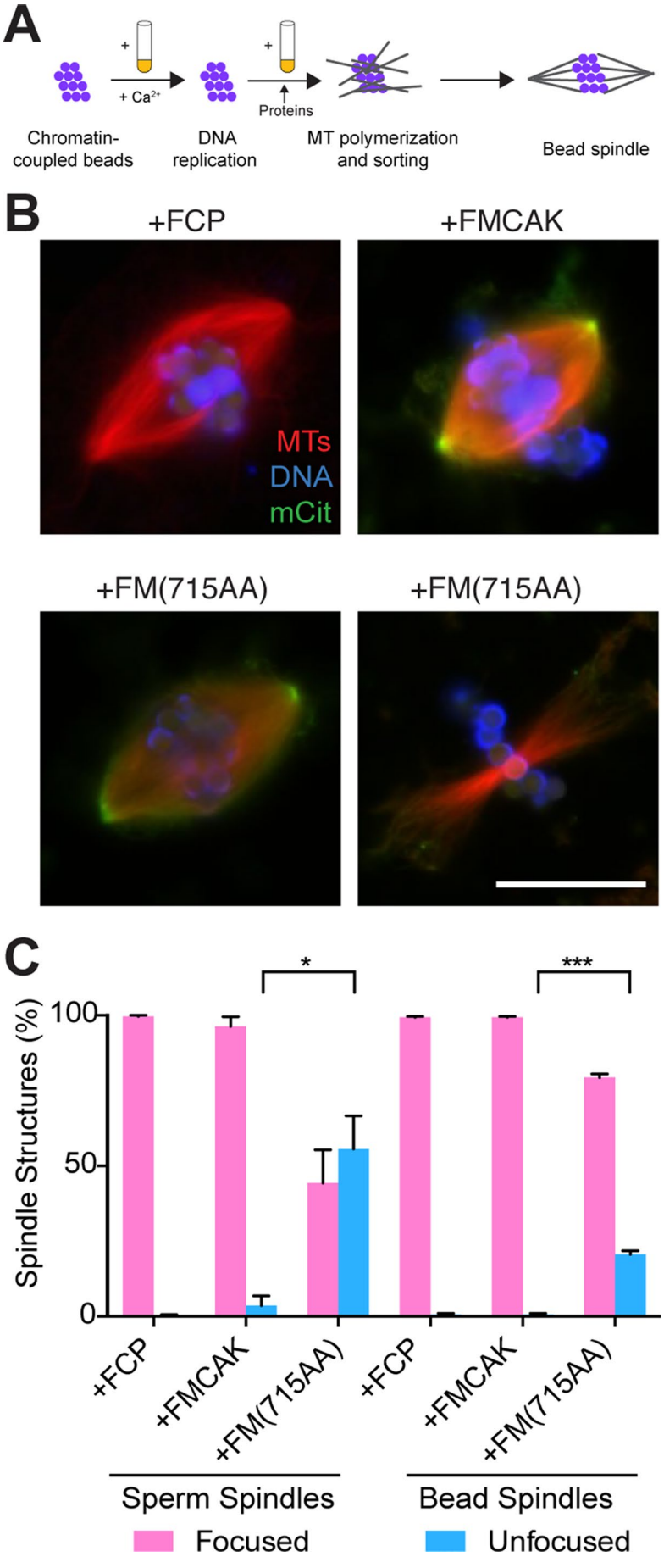

the ΔM+FMCAK control spindles was 2.52 s (95% CI = 2.42–2.63 s) at the poles and 2.27 s (95% CI = 2.16–2.39 s; $p < 0.01$) at the midzone, suggesting that the MTs at the midzone are more dynamic and undergo more catastrophes (Figure 5K). In contrast, EB1 lifetimes at the poles in ΔM+FM(715AA) focused spindles had a much shorter average lifetime of 2.20 s (95% CI = 2.15–2.26 s) compared with ΔM+FMCAK ($p < 0.0001$; Figure 5K). The EB1 comets at the midzone of ΔM+FM(715AA) focused spindles also had a lifetime of 2.18 s (95% CI = 2.02–2.38 s) that was statically indistinguishable from ΔM+FMCAK at the midzone ($p = 0.41$) and statistically identical to ΔM+FM(715AA) at the poles ($p = 0.80$; Figure 5K). The lifetimes of EB1 comets at the pole region in ΔM+FM(715AA) unfocused spindles were further reduced to 2.03 s (95% CI = 1.95–2.12 s) compared with the pole regions in ΔM+FMCAK ($p < 0.0001$) and ΔM+FM(715AA) focused spindles ($p < 0.01$), suggesting a more severe pole defect in these spindles (Figure 5K). In contrast, the lifetime of EB1 comets at the midzone of ΔM+FM(715AA) unfocused spindles (2.19 s; 95% CI = 2.06–2.34 s) was unchanged relative to ΔM+FMCAK ($p = 0.42$) and ΔM+FM(715AA) focused spindles ($p = 0.95$; Figure 5K). The differences in the distribution of tracks were not due to changes in the velocity of the tracks, which were statistically similar under all conditions (Figure 5L and Supplemental Figure S6). Taken together, our results indicate that the E715A/E716A mutation alters the conformation of MCAK that increases its localization to the poles, which increases the MT dynamics, causing the disruption of the polar array that results in unfocused poles.

XCTK2 addition rescues the unfocused-pole phenotype caused by FM(715AA)

The assembly and maintenance of the bipolar spindle structure require a balance between MT dynamics, MT cross-linking, motor forces, and pole-focusing activity (Loughlin *et al.*, 2010). The increased targeting of FM(715AA) to the polar regions of spindles may be disrupting MT dynamics, which in turn tips the balance of forces needed to focus the spindle poles. The kinesin-14 XCTK2 cross-links and slides MTs for proper pole focusing (Walczak *et al.*, 1997, 1998; Mountain *et al.*, 1999; Goshima *et al.*, 2005). Thus we reasoned that the addition of extra XCTK2 might restore pole focusing in the presence of FM(715AA). To test this hypothesis, we added a

FIGURE 4: FM(715AA) can generate unfocused poles in chromatin-bead spindles. (A) *Xenopus* egg extracts containing chromatin-coupled beads were cycled into interphase, supplemented with 100 nM FCP, FMCAK, or FM(715AA), and cycled back into mitosis, and then spindles were assembled. (B) Representative images of spindles in FCP, FMCAK, and FM(715AA) reactions. Images were scaled equivalently except for the MTs in the unfocused spindle in FM(715AA) reactions, in which the MT channel was enhanced to visualize the structure. Scale bar, 20 μm. (C) Quantification of the percentage of spindle structures that are categorized with focused or unfocused spindle poles. Data represent mean ± SD ($n = 3$; 100 structures counted per experiment). *$p < 0.05$, ***$p < 0.001$.

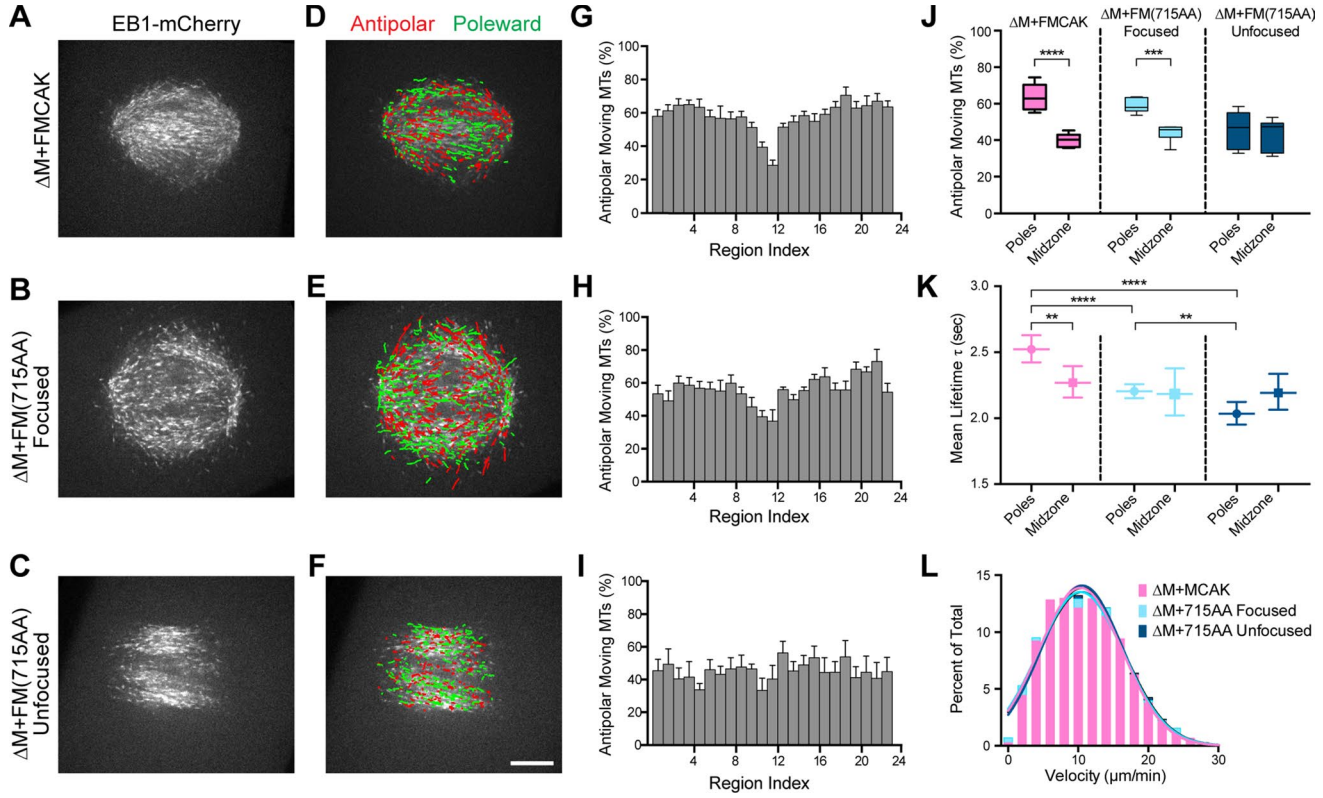

FIGURE 5: FM(715AA) inhibits MT growth from the poles and shortens the lifetime of growing MTs. (A–C) Single-frame confocal images of 0.3 μM EB1-mCherry in a control ΔM+FMCAK spindle, a focused ΔM+FM(715AA) spindle, and an unfocused ΔM+FM(715AA) spindle. Scale bar, 10 μm. (D–F) EB1 comets from time-lapse sequence of spindles in A–C were identified and tracked using plusTipTracker. Tracks were color coded to reflect the direction of growth, in which red indicates antipolar movement and green indicates poleward movement. Tracks were overlaid onto the single-frame image on the left. (G–I) Spindles were divided into 23 regions, and the distributions of tracks were plotted as mean ± SEM of the percentage of antipolar-moving MTs corresponding to the regions in D (7 spindles, 4972 tracks), E (6 spindles, 3696 tracks), and F (6 spindles, 2514 tracks). (J) The average percentage of antipolar-moving EB1 tracks in the two pole regions was calculated and compared with that at the spindle midzone. (K) Lifetimes of EB1 tracks in pole and midzone regions were measured and fitted with a one-phase exponential decay to determine the rate constant K (sec^{-1}), and the average lifetime (τ) of the EB1 comets was determined from K^{-1}. The average lifetime is plotted as mean ± 95% CI. (L) Histogram and Gaussian fit of EB1 track velocities detected in ΔM+FMCAK spindles or ΔM+FM(715AA) spindles with focused or unfocused poles. For details, see Supplemental Figure S5. $^{**}p < 0.01$, $^{***}p < 0.001$, $^{****}p < 0.0001$.

fivefold excess of XCTK2 (100 nM) to MCAK-depleted and FMCAK or FM(715AA) add-back extracts (Figure 6A and Supplemental Figure S7). We found that XCTK2 overaddition reduced the percentage of spindles with unfocused poles in FM(715AA) reactions (7 ± 8%) compared with reactions without added XCTK2 (32 ± 13%; $p < 0.05$; Figure 6B). These results suggest that FM(715AA) tips the balance between proper MT dynamics and pole-focusing activities but that the balance can be restored by the presence of excess MT cross-linking and sliding activity. In ΔM+FM(715AA) spindles, excess XCTK2 may cross-link the shorter and more dynamic MTs at the pole region or cross-link MTs in the overlapping region between the polar and barrel array, preventing the decoupling of the polar array from the barrel array (Yang *et al.*, 2008).

The S719 phosphorylation-mimic mutation S719E disrupts CT binding to MD and mimics the conformation induced by the 715AA mutation

Our previous work showed that Aurora A phosphorylates S719, which stimulates spindle assembly and increases the targeting of MCAK to spindle poles in Ran-GTP spindles (Zhang *et al.*, 2008). Hence one model for how FM(715AA) may affect spindle assembly is by increasing the phosphorylation of S719, which results in a conformational change in MCAK that leads to increased pole targeting and defects in spindle pole focusing. Consistent with this idea, phosphorylation-site prediction by KinasePhos 2.0 (Wong *et al.*, 2007) indicates that S719 has a higher probability of being phosphorylated in the 715AA mutant. If this model is correct, then we reasoned that phosphorylation at S719 or a phosphomimetic mutation at this site would cause a change in MCAK conformation and result in spindle pole defects during spindle assembly. Using GST pull-down experiments, we found that, like GST-CT(715AA), GST-CT(S719E) was not able to bind to MD, whereas GST-CT(S719A) could bind, but in reduced amounts (Supplemental Figure S8). We also tested whether the S719E mutation altered the conformation of MCAK by constructing a FRET biosensor of the S719E mutant, FM(S719E). As a control, we generated FM(S719A), which should not undergo a conformational change or disrupt pole structure in spindle assembly reactions if our hypothesis is correct. Similar to the results with FM(715AA), FM(S719E) had higher FRET than FMCAK, whereas FM(S719A) had a decreased FRET emission (Figure 7A). Together these results suggest that the phosphomimetic mutation at S719 reduces the binding between the CT and MD and allows

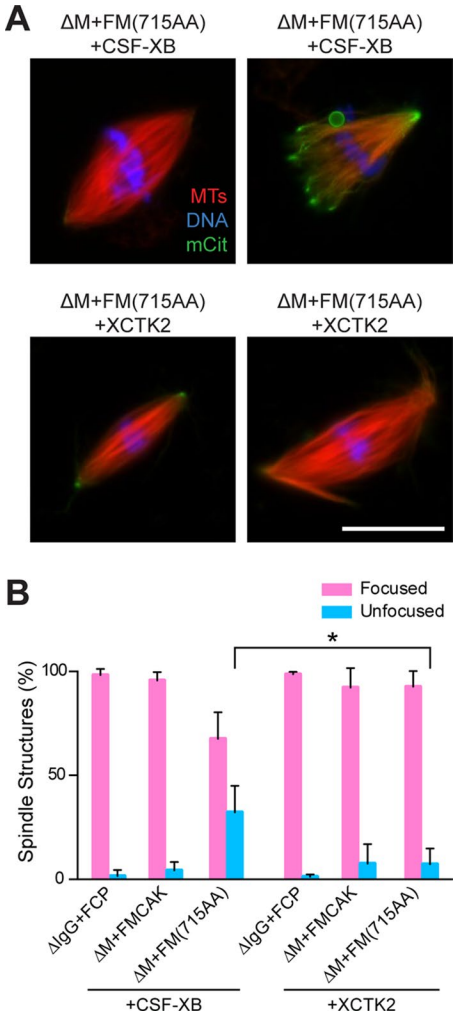

FIGURE 6: XCTK2 addition rescues the unfocused-pole phenotype in spindles reconstituted with FM(715AA). (A) Representative images of spindles in MCAK-depleted *Xenopus* egg extracts that were reconstituted with 100 nM FCP, FMCAK, or FM(715AA) together with a fivefold excess of XCTK2 (100 nM) or equal volume of control buffer (CSF-XB). Scale bar, 20 μm. (B) Quantification of the percentage of spindle structures categorized as focused or unfocused spindles. Data represent mean ± SD ($n = 3$; 100 structures counted per experiment). *$p < 0.05$.

MCAK to adopt a more "closed" conformation, similar to that seen with FM(715AA).

Given that the FRET of FM(S719E) was also increased relative to FMCAK, we asked whether FM(S719E) mirrors FM(715AA) in inducing spindles with unfocused poles in our extract assay. FMCAK or mutant proteins were added to MCAK-depleted extracts and assayed for spindle assembly (Figure 7B). Addition of FM(S719E) resulted in an increased percentage of spindles with unfocused poles (31 ± 16%) relative to FMCAK ($p < 0.05$) and was similar to that seen with FM(715AA) (42 ± 15%, $p = 0.40$; Figure 7C). In contrast, the majority of structures with FM(S719A) add-back were bipolar spindles with focused poles (82 ± 4%). Taken together, these results indicate that, similar to the 715AA mutation, a phosphomimetic mutation at S719 not only causes a conformational change in MCAK but also induces spindles with unfocused poles, which may suggest a similar change in conformation and defect in spindle assembly.

FM(715AA) induces the unfocused-pole phenotype due to its altered conformation instead of an increase in phosphorylation of S719

To examine the causal relationship between the altered conformation, phosphorylation of S719, and the unfocused-pole phenotype, we generated a triple mutant, FM(715AA/S719A), and tested whether it affected MCAK conformation and caused the unfocused-pole phenotype (Figure 7, D–F). We found that FM(715AA/S719A) had a FRET emission profile that was statistically identical to that of FM(715AA) ($p = 0.54$), indicating the 715AA mutation is dominant for controlling MCAK conformation (Figure 7D). If the FM(715AA) mutant only affects spindle assembly by promoting the phosphorylation of S719 but not through a conformational change, we reasoned that 715AA/S719A mutation would not cause the pole defects in spindle assembly reactions. Alternatively, if the altered conformation induced by phosphorylation at S719 or 715AA is required for the unfocused-pole phenotype, we predict that FM(715AA/S719A) should result in defects in spindle pole focusing. Indeed, replacement of endogenous MCAK with FM(715AA/S719A) resulted in spindles with unfocused poles (71 ± 1%; Figure 7, E and F), suggesting that phosphorylation of S719 in the FM(715AA) protein is not required for the unfocused-pole phenotype. Instead, these findings argue that the change in conformation, which can occur by phosphorylation of S719 or by the E715A/E716A mutations, leads to the defects in spindle pole focusing.

DISCUSSION

Here we propose that the subcellular pools of MCAK are tightly controlled by multiple kinases that phosphorylate different MCAK domains to regulate its conformation, which in turn regulates its subspindle targeting and activity during spindle assembly (Figure 8A). We show that the 715AA mutation and S719 phosphorylation cause similar conformational changes in MCAK, which lead to increased pole targeting. This results in increased MT dynamicity at the poles, which tips the balance of pole-focusing motor activity and results in pole-focusing defects during spindle assembly (Figure 8B). These findings elucidate a role for MCAK at the spindle poles and provide the basis for a mechanism by which regional regulation of MT dynamics by kinases is critical to ensure proper spindle pole formation.

The far C-terminus of MCAK regulates its conformation

Our data, as well as those of others, highlight the idea that the MCAK CT interacts with MD to regulate its subcellular targeting and activity (Moore and Wordeman, 2004; Moore *et al.*, 2005; Hertzer *et al.*, 2006; Ems-McClung *et al.*, 2007, 2013). We show that the EEXXS motif (residues 715–719) in the far CT plays an important role in MCAK conformation, which affects function. This is supported by the crystal structure of the MD dimer from CgMCAK bound to a single peptide of the last 25 amino acids of the CT (Talapatra *et al.*, 2015). In this structure, E711 and E712 (E715 and E716 in *Xenopus* MCAK) bind the interface between the two motor and proximal neck domains, stabilizing dimerization. This suggests that the CT of MCAK is flexible, which allows it to fold back toward the motor domain. In addition, S715 (S719 in *Xenopus* MCAK) is positioned toward the motor domain in the crystal structure, which is consistent with our idea that phosphorylation at S715/S719 could be a useful strategy for regulating MCAK conformation.

Here we propose an expanded model for MCAK conformation. In solution, the far CT stabilizes MCAK dimerization by folding back toward the motor domain. This configuration is prohibitive to lattice binding because of the steric hindrance of the neck domains pointing in a position perpendicular to the longitudinal

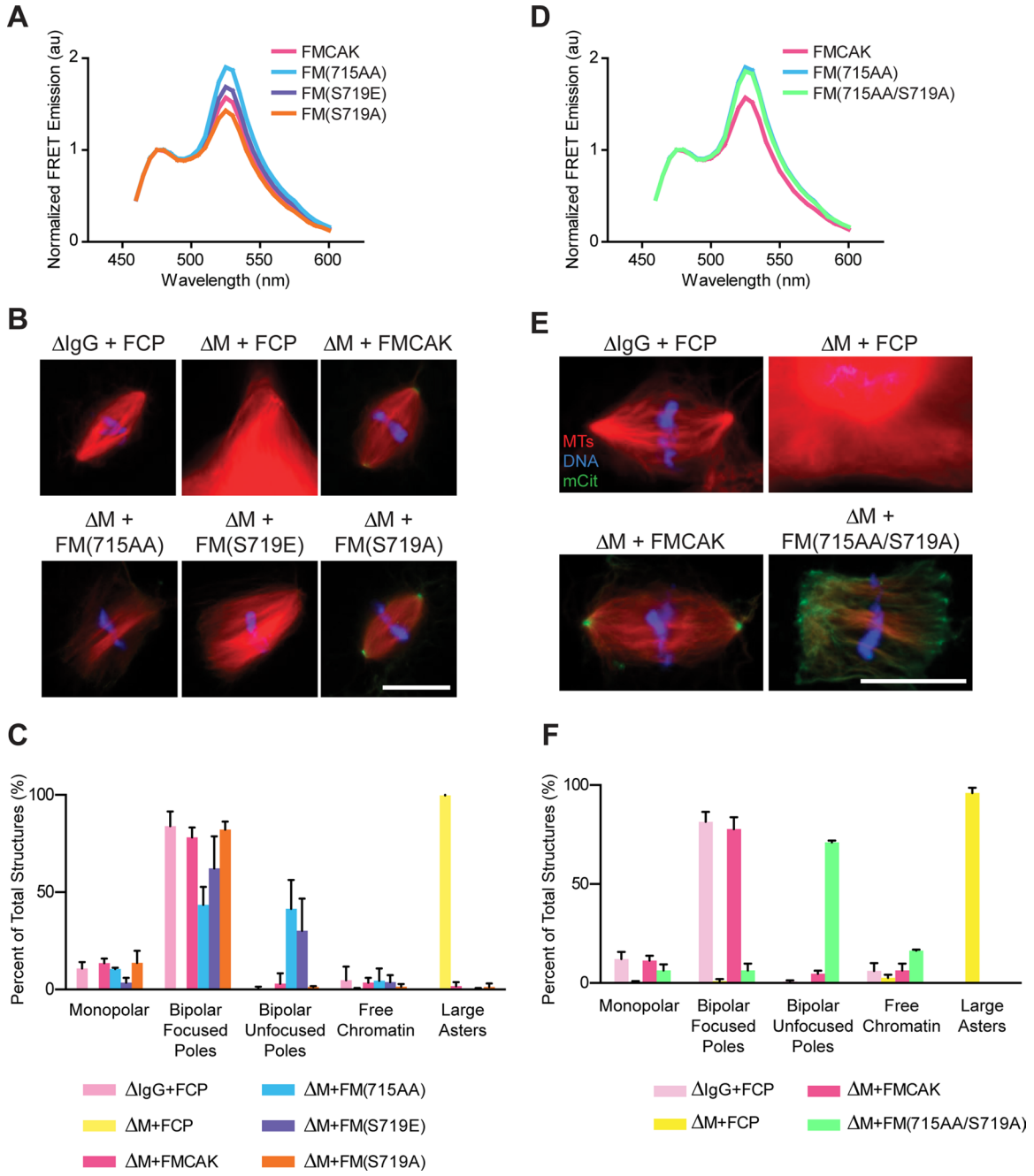

FIGURE 7: FM(715AA) induces the unfocused-pole phenotype due to its altered conformation. (A) The phosphomimetic S719E and dephospho S719A mutations were made in FMCAK and their conformation measured using FRET by exciting mCerulean at 433 nm and measuring the emission from 460 to 600 nm. Data represent the mean of at least three experiments. (B) Representative images of spindles assembled in MCAK-depleted extracts that were reconstituted with 100 nM FCP, FMCAK, FM(715AA), FM(S719E), or FM(S719A). Scale bar, 20 μm. (C) Quantification of the MT structures in B. Data represent mean ± SD of three separate extracts in which 100 structures were counted per condition. (D) FRET emission of FM(715AA/S719A) compared with FMCAK and FM(715AA). Note that both curves nearly overlap. (E) Representative images of spindles reconstituted with 100 nM FCP, FMCAK, or FM(715AA/S719A). Scale bar, 20 μm. (F) Quantification of the MT structures in E. Data represent mean ± SD of three separate extracts in which 100 structures were counted per condition.

axis of the MT (Moore and Wordeman, 2004; Talapatra *et al.*, 2015). We propose that the 715AA/S719E mutations release the far CT from the motor domains, which brings the far CT in closer proximity to the NT, resulting in higher FRET (Figure 8B). This increased conformational flexibility might increase lattice binding to MTs at the spindle pole. Furthermore, we propose that the conformational changes induced by the 715AA and S719E mutations are distinct from the conformational changes we observed in our previous work when MCAK binds to the MT lattice or is phosphorylated by Aurora B (Ems-McClung *et al.*, 2013). Understanding the detailed MCAK conformation will require elucidation of the full-length structure.

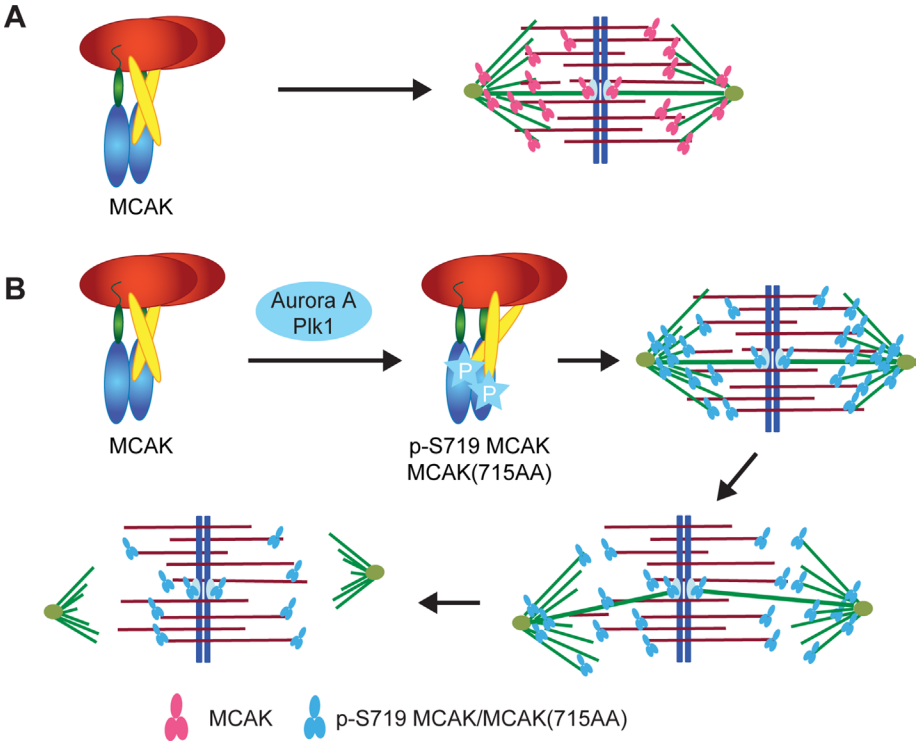

FIGURE 8: Model for how the MCAK conformation alters subspindle targeting and generates spindles with unfocused poles. (A) MCAK displays a closed conformation in solution and is localized to kinetochores, spindle poles, and plus tips of MTs. (B) MCAK conformation is modulated through phosphorylation at S719 by either Aurora A or Plk1 kinase. E715A/E716A mutation in the far C-terminus of MCAK mimics this conformational change, resulting in a more "closed" conformation that brings the CT closer to the NT. This altered conformation of MCAK causes increased localization at the polar regions, which shortens MTs and reduces MT growth from the poles. Reducing MT length and number at the pole disrupts the polar array or may decouple the MT polar array from the barrel array, leading to spindles with unfocused poles.

Pole-focusing defects likely result from increased targeting to spindle poles

How do MCAK(715AA) and MCAK(S719E) generate spindles with unfocused poles in extracts? We found that the 715AA mutation did not statistically increase MT depolymerization activity compared with wild-type MCAK. This is supported by previous studies of ours and from the Welburn group, which show that S719E/S715E have similar MT depolymerization activity as wild-type MCAK (Zhang *et al.*, 2008; Talapatra *et al.*, 2015). Conversely, another recent study showed that CgMCAK(S715E) has slightly increased MT depolymerization activity in vitro, which we believe is not sufficient to explain the unfocused-pole phenotype under physiological conditions in our extract experiments (Shao *et al.*, 2015).

Our present findings favor the idea that a change in MCAK conformation causes increased targeting of MCAK to spindle poles, resulting in local changes in MT depolymerization activity. Although the increased localization of the MCAK(715AA) mutant seems like a relatively small increase, mathematical modeling studies show that increasing MT catastrophe frequency is the most effective means for reducing the average length of microtubules at steady state (Verde *et al.*, 1992; Loughlin *et al.*, 2010). Therefore only a small change in localization could be amplified to have a larger effect on MT length. Our results also highlight the idea that locally increasing MCAK activity in the spindle does not require a change in its enzymatic MT depolymerization activity but instead simply a change in the amount of targeting. In support of this idea, several studies show that MCAK CT phosphorylation by different kinases affects protein targeting (Zhang *et al.*, 2008, 2011; Shao *et al.*, 2015). A recent study shows that an S715 phosphospecific antibody stains centrosomes in addition to kinetochores, and overexpression of MCAK(S715E) in cells causes multipolar spindles, which supports a cellular role for S715 phosphorylation at spindle poles (Shao *et al.*, 2015). It is not known, however, how the CT mutants increase MCAK targeting to the poles. It is reported that MCAK(S715E) displays increased MT lattice-binding affinity, resulting in a tail that follows the EB1 comet (Shao *et al.*, 2015; Talapatra *et al.*, 2015). MCAK is likely enriched by EB1 to the nascent MT plus ends emanating from the centrosomes/spindle poles. Therefore one possible explanation for the shorter MT lifetimes and increased depolymerization activity at the pole region is that the increased protein targeting of 715AA/S719E on the lattice makes it less likely for a shrinking MT to be rescued.

Proposed mechanism by which MCAK(715AA) generates spindles with unfocused poles

The nonkinetochore MTs in the meiotic *Xenopus* spindle comprise short MTs that can be subdivided into a barrel array of antiparallel MTs in the center and a polar array at each side (Yang *et al.*, 2007, 2008). MT cross-linking proteins, such as dynein, are proposed to couple the polar and barrel MTs in the overlapping regions (Yang *et al.*, 2008). Our data support the idea that MCAK may also be important in coupling these two arrays by precisely regulating MT dynamics of the polar array. We propose that FM(715AA) generates unfocused poles by preferentially targeting and depolymerizing MTs in the polar array, which results in fewer and shorter MTs, which cannot be coupled with the barrel array (Figure 8B). This model is consistent with our finding that FM(715AA) caused a reduced frequency of unfocused poles in bead spindles. Bead spindles also contain one barrel array and two polar arrays, but the contribution of MTs in the polar arrays is smaller than in sperm-induced spindles (Yang *et al.*, 2008). This explains the reduced number of unfocused spindles in bead spindle assembly reactions and indicates that FM(715AA) preferentially destabilizes MTs in the polar array.

Overall our data favor the idea that conformational changes of MCAK make a major contribution to the regulation of MCAK subspindle localization and function. This conformation needs to be tightly regulated by phosphorylation at distinct sites in the protein. Aurora B phosphorylates MCAK in the neck, which results in an open conformation of MCAK (Ems-McClung *et al.*, 2013) that inhibits the MT depolymerization activity of MCAK; Aurora A and Plk1 phosphorylate MCAK in the far CT, which results in a more "closed" conformation that increases the protein targeting to spindle poles. By using this mechanism, the precise temporal and spatial regulation of these kinases can have a profound effect on local MT depolymerization activity.

MATERIALS AND METHODS

Protein expression and purification

GST-tagged proteins were cloned into pGEX3* using PCR and expressed and purified as described previously (Ems-McClung *et al.*, 2004). GST-CT comprises *Xenopus* MCAK amino acids 593–730, GST-CTΔ14 consists of amino acids 593–717, GST-CTΔ27 comprises amino acids 593–703, GST-CTΔ62 consists of amino acids 593–668, and CTΔ120 comprises amino acids 593–610. Enhanced GFP, mCerulean, mCitrine, and FCP were expressed as hexahistidine-tagged proteins as previously described (Ems-McClung *et al.*, 2013). GFP-tagged minimal domain MCAK (GMD), XCTK2, and MCAK FRET reporter proteins (FMCAK) were expressed in Sf-9 or HighFive insect cells (Invitrogen, Waltham, MA) and purified using conventional chromatography (Walczak *et al.*, 1997; Hertzer *et al.*, 2006; Ems-McClung *et al.*, 2013). Point mutations (E715AE716A [715AA], S719E, S719A, and 715AA/719A) were generated using the QuikChange Site-directed Mutagenesis System (Stratagene, La Jolla, CA) as described previously (Ems-McClung *et al.*, 2004). All clones were verified by sequencing. Protein concentrations were determined using densitometry compared with bovine serum albumin (BSA) on colloidal Coomassie Blue–stained SDS–polyacrylamide gels. MCAK concentrations are expressed as monomer amounts.

Glutathione pull-down assays

Glutathione pull-down assays were performed by adding 35 µl of 70 pmol GMD and 210 pmol GST or GST-CT protein in 1 mM MgATP, 140 mM KCl, and BRB49 (49 mM 1,4-piperazinediethanesulfonic acid, pH 6.8, 1 mM $MgCl_2$, 1 mM ethylene glycol tetraacetic acid, 1 mM dithiothreitol) to 65 µl of a bead slurry containing 30 µl of settled Glutathione Sepharose 4B (GE Healthcare, Pittsburgh, PA) in 1 mg/ml gelatin, 1 mM MgATP, and BRB49. Bead–protein mixes were incubated at 4°C with rotation for 45 min and centrifuged, and the supernatant was saved as the soluble fraction. The beads were washed twice with 10 volumes of BRB49 and twice with 10 volumes of BRB49 and 0.1% (vol/vol) NP-40. The bound proteins were eluted with SDS–PAGE sample buffer. Equivalent amounts of input, bound, and soluble fractions were electrophoresed on 10% (vol/vol) SDS–PAGE gels and stained with colloidal Coomassie Blue. The amount of GMD in each fraction was quantified by densitometry compared with a known amount of BSA run on the same gel using ImageJ (National Institutes of Health, Bethesda, MD). The amount of GMD bound to the GST-CT proteins was corrected for the nonspecific amount of GMD that bound to GST alone. Statistics were performed in Excel (Microsoft, Redmond, WA) using the *F* test for variance and the two-tailed Student's *t* test. Results were considered significant if $p < 0.05$.

FRET and FLIM

For FRET, equal molar amounts of mCerulean and mCitrine, FCP, or MCAK FRET reporter proteins were excited at 433 nm, and the emission was measured in 0.5-nm steps from 445 to 600 nm in a Perkin Elmer LS 50B fluorometer or measured in 5-nm steps from 460 to 600 nm in a BioTek Synergy H1 microplate reader. FRET assays in the fluorometer were performed with 125 nM protein, 20 mM KCl, 2 mM MgATP, and BRB49 (Ems-McClung *et al.*, 2013), and assays in the microplate reader were performed with 100 nM protein, 20 mM KCl, 2 mM MgATP, and 0.2 µg/µl casein in BRB49. The emission was normalized to 475 nm (the peak emission of mCerulean) using Excel, and the average emission was calculated and graphed in Prism (GraphPad, La Jolla, CA).

FLIM was performed with biotin-X-rhodamine–labeled GMPCPP (guanylyl-(α,β)-methylene-diphosphonate)/paclitaxel–stabilized MTs adhered to #1.5 glass coverslips silanized with biotin–polyethylene glycol as described previously (Ems-McClung *et al.*, 2013), except that FMCAK proteins were diluted to 250 nM in 20 mM KCl, 5 mM AMPPNP (adenylyl-imidodiphosphate), 10 µM paclitaxel, and BRB49, brought to room temperature, and then introduced into the chamber. Images were acquired on a Leica SP5 laser scanning confocal microscope equipped with a 63×/1.2 numerical aperture (NA) HCX PL APO CS water objective (Leica, Buffalo Grove, IL) with an attached Becker and Hickl multidimensional time-correlated photon counting system, and lifetimes were measured using a custom-built MATLAB (MathWorks, Natick, MA) algorithm as described (Ems-McClung *et al.*, 2013). Lifetimes were exported in tab-delimited files and assembled in Prism for frequency distribution analysis and graphing. Statistical differences were determined using an *F* test of the Gaussian distribution of the means in Prism.

Microtubule EC_{50} assays

The effective concentration of MCAK at which 50% of the MTs were depolymerized (EC_{50}) was determined as described (Hertzer *et al.*, 2006). Briefly, 1 µM GMPCPP-stabilized MTs were incubated with 0–30 nM FMCAK or FM(715AA) in 20 mM KCl, 2 mM MgATP, 0.2 µg/µl casein, and BRB49 for 30 min and sedimented at 45,000 rpm at 22°C to separate the soluble tubulin and tubulin polymer. Equivalent amounts of soluble and polymer fractions were electrophoresed on 10% SDS–PAGE and stained with colloidal Coomassie Blue. The best-fit EC_{50} for each protein was determined by densitometry and the four-parameter logistic equation in Prism from four independent experiments (Ems-McClung *et al.*, 2007). Statistical differences were determined between the best-fit EC_{50} means using an *F* test in Prism.

Spindle assembly in *Xenopus* egg extracts

Cytostatic factor (CSF)–arrested *Xenopus laevis* egg extracts were prepared as described (Murray, 1991). MCAK immunodepletions and add-back of recombinant proteins were performed as described (Zhang *et al.*, 2007). Rhodamine-labeled tubulin was added to all extracts to a final concentration of 30 µg/ml, and demembranated sperm nuclei were added at 300/µl to the extracts. FCP, FMCAK, or mutant protein was added at a final concentration of 100 nM to the extracts with the second CSF addition and incubated for 70 min for spindle assembly. For XCTK2 rescue experiments, 100 nM XCTK2 or control CSF-XB buffer was added to extracts along with the FMCAK addition. After spindle assembly, samples were pelleted onto coverslips as described (Desai *et al.*, 1999a). Chromatin bead spindle assembly was carried out as described (Heald *et al.*, 1996). Chromatin or chromatin/MT structures were counted from at least three independent extracts in which ~100 structures were counted per reaction. Western blots were carried out for each extract to confirm that equal amounts of protein were added to the extracts.

For Western analysis, extract was diluted 1:10 with sample buffer, and equal amounts of each reaction were electrophoresed on 10% (vol/vol) SDS–PAGE gels and transferred to nitrocellulose. Primary antibodies were used at 0.5 µg/ml for rabbit anti-NT2-xMCAK (Walczak *et al.*, 1996) and 1:5000 for mouse DM1α anti-tubulin antibody (Sigma-Aldrich, St. Louis, MO). Secondary antibodies were used at 1 µg/ml for goat anti-rabbit– and sheep anti-mouse–linked horseradish peroxidase (Invitrogen). Blots were developed with SuperSignal West Pico Chemiluminescent Substrate (Pierce).

Imaging and quantification of fluorescence intensity

Single-plane images were collected on a Nikon (Melville, NY) Eclipse 90i using a 40× Plan Apo (NA 1.0) objective with a CoolSnap HQ charge-coupled device (CCD) camera (Photometrics, Tucson, AZ) that

was controlled by MetaMorph (Molecular Devices, Sunnyvale, CA). All images in each experiment were taken with the same exposure time and scaled equivalently unless otherwise noted. Images were processed in Fiji (http://imagej.net/Fiji) and assembled in Illustrator (Adobe, San Jose, CA).

We wrote a custom MATLAB code to assess the targeting affinity of proteins on the entire spindle. Briefly, a box was manually drawn around the edges of the spindle, and each spindle was subdivided into 100 bins to normalize the spindle lengths. The fluorescent signal in each channel from pole to pole was collected and averaged per bin. To minimize the effects due to normal variability of extract spindles in MT density and protein localization, a ratio of the protein to MT intensity (fluorescein isothiocyanate/Texas Red ratio) was calculated (Cai *et al.*, 2010). Data plotted represent the mean ± SD in which 10–20 spindle structures were analyzed per condition in three independent extracts. To compare the significance of the difference in protein targeting, a Student's *t* test of the protein to MT intensity ratio across the spindle in each bin was performed (Wilbur and Heald, 2013). Differences were considered statistically significant if $p < 0.05$.

Live imaging

Spindles were assembled in depleted, cycled extracts without rhodamine-tubulin. At the time of the second CSF addition, 100 nM of the indicated recombinant proteins were added back to the extract along with 0.33 µM 6His-hEB1-mCherry. Movies of EB1-mCherry or Alexa 594–EB1 were collected on a Nikon TE2000U microscope platform with a 100× Plan Apo 1.4 NA lens (Nikon). Illumination was with a 75-mW krypton/argon laser through a Yokogawa CSU-10 spinning-disk confocal head (PerkinElmer Life and Analytical Sciences, Boston, MA). Images were acquired at 2- or 5-s intervals and collected with a Cascade-II electron-multiplying CCD camera (Photometrics). Microscope acquisition was controlled with NIS Elements software (Nikon). Movies were realigned using a Fiji plug-in (Rigid Registration) to correct for the rotation and drift of spindles during imaging.

EB1 tracking analysis

To detect and track EB1 comets, images were analyzed using plusTipTracker (Applegate *et al.*, 2011) with the following parameters: maximum gap length, 0; minimum track length, 3 frames; backward angle, 10; forward angle, 30; search radius range, 1.5–2.7 pixels; fluctuation radius (pixels), 1; and maximum shrinkage factor, 1.5. The parameters were optimized by checking tracks manually with a cutoff >80% accuracy. After detection, EB1 distribution and angular orientation were calculated using a custom-written MATLAB code. Briefly, the positions of the two spindle poles were input manually, and the spindle was rotated to make the long axis horizontal. We drew a line equidistant between the two poles and then calculated the percentage of tracks in each half-spindle that moved toward (poleward) or away from (antipolar) the spindle pole. In each half-spindle, the orientation that a track that moved toward (poleward) or away from (antipolar) was determined based on the angle between the first comet and the average of the rest of the comets within that track. The spindle was equally divided into 23 bins across the long axis of the spindle (Yang *et al.*, 2008), and the localization of each comet was assigned based on its coordinate in the first frame. The number of EB1 comets and the percentage of antipolar-moving MTs were determined at each bin and plotted as the mean ± SEM per bin. The spindle midzone was defined as the center three bins, and the poles were defined as the terminal three bins. The data from the poles were averaged to correct for the asymmetrical MT distribution in the two halves of the spindle and compared with that at the spindle midzone with the Student *t* test. All data were plotted in MATLAB or Prism.

We used *x*, *y*-coordinates generated by plusTipTracker to analyze the velocity and lifetimes of EB1 tracks. Frame-to-frame velocity was determined by dividing the distance a comet tracked by time interval, and the velocity of each track was averaged from all the frame-to-frame velocities (Applegate *et al.*, 2011). The distribution of velocities in each spindle type was plotted as a histogram in MATLAB and fitted to a Gaussian distribution in Prism. Comet lifetime is determined as the amount of time a comet persists before it disappeared. The position assignment of comet lifetime at the pole or midzone regions was as described earlier. The lifetimes at the pole or midzone were fitted with a one-phase decay nonlinear regression, and the mean lifetime τ (s) was compared using its reciprocal, the phase constant K (s^{-1}), in Prism. The mean lifetime τ with 95% confidence interval was plotted.

ACKNOWLEDGMENTS

We thank Ryoma Ohi for the EB1-mCherry constructs. We give special thanks to Jim Powers for assistance with the imaging. We thank Rebecca Heald, Sid Shaw, and members of the Walczak lab for helpful discussions on the project and Lesley Weaver for comments on the manuscript. This work was funded by National Institutes of Health Grant GM059618 to C.E.W. The Indiana University Light Microscopy Imaging Center is supported in part by the Office of Vice Provost for Research at Indiana University.

REFERENCES

Andrews PD, Ovechkina Y, Morrice N, Wagenbach M, Duncan K, Wordeman L, Swedlow JR (2004). Aurora B regulates MCAK at the mitotic centromere. Dev Cell 6, 253–268.

Applegate KT, Besson S, Matov A, Bagonis MH, Jaqaman K, Danuser G (2011). plusTipTracker: quantitative image analysis software for the measurement of microtubule dynamics. J Struct Biol 176, 168–184.

Cai S, Weaver LN, Ems-McClung SC, Walczak CE (2010). Proper organization of microtubule minus ends is needed for midzone stability and cytokinesis. Curr Biol 20, 880–885.

Cooper JR, Wagenbach M, Asbury CL, Wordeman L (2010). Catalysis of the microtubule on-rate is the major parameter regulating the depolymerase activity of MCAK. Nat Struct Mol Biol 17, 77–82.

Desai A, Murray A, Mitchison TJ, Walczak CE (1999a). The use of Xenopus egg extracts to study mitotic spindle assembly and function in vitro. Methods Cell Biol 61, 385–412.

Desai A, Verma S, Mitchison TJ, Walczak CE (1999b). Kin I kinesins are microtubule-destabilizing enzymes. Cell 96, 69–78.

Domnitz SB, Wagenbach M, Decarreau J, Wordeman L (2012). MCAK activity at microtubule tips regulates spindle microtubule length to promote robust kinetochore attachment. J Cell Biol 197, 231–237.

Ems-McClung SC, Hainline SG, Devare J, Zong H, Cai S, Carnes SK, Shaw SL, Walczak CE (2013). Aurora B inhibits MCAK activity through a phosphoconformational switch that reduces microtubule association. Curr Biol 23, 2491–2499.

Ems-McClung SC, Hertzer KM, Zhang X, Miller MW, Walczak CE (2007). The interplay of the N- and C-terminal domains of MCAK control microtubule depolymerization activity and spindle assembly. Mol Biol Cell 18, 282–294.

Ems-McClung SC, Zheng Y, Walczak CE (2004). Importin α/β and Ran-GTP regulate XCTK2 microtubule binding through a bipartite nuclear localization signal. Mol Biol Cell 15, 46–57.

Goshima G, Nedelec F, Vale RD (2005). Mechanisms for focusing mitotic spindle poles by minus end-directed motor proteins. J Cell Biol 171, 229–240.

Heald R, Tournebize R, Blank T, Sandaltzopoulos R, Becker P, Hyman A, Karsenti E (1996). Self-organization of microtubules into bipolar spindles around artificial chromosomes in Xenopus egg extracts. Nature 382, 420–425.

Hertzer KM, Ems-McClung SC, Kline-Smith SL, Lipkin TG, Gilbert SP, Walczak CE (2006). Full-length dimeric MCAK is a more efficient microtubule depolymerase than minimal domain monomeric MCAK. Mol Biol Cell 17, 700–710.

Honnappa S, Gouveia SM, Weisbrich A, Damberger FF, Bhavesh NS, Jawhari H, Grigoriev I, van Rijssel FJ, Buey RM, Lawera A, *et al*. (2009). An EB1-binding motif acts as a microtubule tip localization signal. Cell 138, 366–376.

Hunter AW, Caplow M, Coy DL, Hancock WO, Diez S, Wordeman L, Howard J (2003). The kinesin-related protein MCAK is a microtubule depolymerase that forms an ATP-hydrolyzing complex at microtubule ends. Mol Cell 11, 445–457.

Kline-Smith SL, Khodjakov A, Hergert P, Walczak CE (2004). Depletion of centromeric MCAK leads to chromosome congression and segregation defects due to improper kinetochore attachments. Mol Biol Cell 15, 1146–1159.

Lan W, Zhang X, Kline-Smith SL, Rosasco SE, Barrett-Wilt GA, Shabanowitz J, Hunt DF, Walczak CE, Stukenberg PT (2004). Aurora B phosphorylates centromeric MCAK and regulates its localization and microtubule depolymerization activity. Curr Biol 14, 273–286.

Loughlin R, Heald R, Nedelec F (2010). A computational model predicts Xenopus meiotic spindle organization. J Cell Biol 191, 1239–1249.

Maney T, Hunter AW, Wagenbach M, Wordeman L (1998). Mitotic centromere-associated kinesin is important for anaphase chromosome segregation. J Cell Biol 142, 787–801.

Maney T, Wagenbach M, Wordeman L (2001). Molecular dissection of the microtubule depolymerizing activity of mitotic centromere-associated kinesin. J Biol Chem 276, 34753–34758.

Matov A, Applegate K, Kumar P, Thoma C, Krek W, Danuser G, Wittmann T (2010). Analysis of microtubule dynamic instability using a plus-end growth marker. Nat Methods 7, 761–768.

Montenegro Gouveia S, Leslie K, Kapitein LC, Buey RM, Grigoriev I, Wagenbach M, Smal I, Meijering E, Hoogenraad CC, Wordeman L, *et al*. (2010). In vitro reconstitution of the functional interplay between MCAK and EB3 at microtubule plus ends. Curr Biol 20, 1717–1722.

Moore AT, Rankin KE, von Dassow G, Peris L, Wagenbach M, Ovechkina Y, Andrieux A, Job D, Wordeman L (2005). MCAK associates with the tips of polymerizing microtubules. J Cell Biol 169, 391–397.

Moore A, Wordeman L (2004). C-terminus of mitotic centromere-associated kinesin (MCAK) inhibits its lattice-stimulated ATPase activity. Biochem J 383, 227–235.

Mountain V, Simerly C, Howard L, Ando A, Schatten G, Compton DA (1999). The kinesin-related protein, HSET, opposes the activity of Eg5 and cross-links microtubules in the mammalian mitotic spindle. J Cell Biol 147, 351–366.

Murray AW (1991). Cell cycle extracts. Methods Cell Biol 36, 581–605.

Ohi R, Sapra T, Howard J, Mitchison TJ (2004). Differentiation of cytoplasmic and meiotic spindle assembly MCAK functions by Aurora B-dependent phosphorylation. Mol Biol Cell 15, 2895–2906.

Ovechkina Y, Wagenbach M, Wordeman L (2002). K-loop insertion restores microtubule depolymerizing activity of a "neckless" MCAK mutant. J Cell Biol 159, 557–562.

Rizk RS, Bohannon KP, Wetzel LA, Powers J, Shaw SL, Walczak CE (2009). MCAK and paclitaxel have differential effects on spindle microtubule organization and dynamics. Mol Biol Cell 20, 1639–1651.

Shao H, Huang Y, Zhang L, Yuan K, Chu Y, Dou Z, Jin C, Garcia-Barrio M, Liu X, Yao X (2015). Spatiotemporal dynamics of Aurora B-PLK1-MCAK signaling axis orchestrates kinetochore bi-orientation and faithful chromosome segregation. Sci Rep 5, 12204.

Talapatra SK, Harker B, Welburn JPI (2015). The C-terminal region of the motor protein MCAK controls its structure and activity through a conformational switch. eLife 4, e06421.

Tirnauer JS, Salmon ED, Mitchison TJ (2004). Microtubule plus-end dynamics in Xenopus egg extract spindles. Mol Biol Cell 15, 1776–1784.

Verde F, Dogterom M, Stelzer E, Karsenti E, Leibler S (1992). Control of microtubule dynamics and length by cyclin A- and cyclin B-dependent kinases in Xenopus egg extracts. J Cell Biol 118, 1097–1108.

Walczak CE, Gan EC, Desai A, Mitchison TJ, Kline-Smith SL (2002). The microtubule-destabilizing kinesin XKCM1 is required for chromosome positioning during spindle assembly. Curr Biol 12, 1885–1889.

Walczak CE, Heald R (2008). Mechanisms of mitotic spindle assembly and function. Int Rev Cytol 265, 111–158.

Walczak CE, Mitchison TJ, Desai A (1996). XKCM1: a Xenopus kinesin-related protein that regulates microtubule dynamics during mitotic spindle assembly. Cell 84, 37–47.

Walczak CE, Verma S, Mitchison TJ (1997). XCTK2: a kinesin-related protein that promotes mitotic spindle assembly in Xenopus laevis egg extracts. J Cell Biol 136, 859–870.

Walczak CE, Vernos I, Mitchison TJ, Karsenti E, Heald R (1998). A model for the proposed roles of different microtubule-based motor proteins in establishing spindle bipolarity. Curr Biol 8, 903–913.

Wilbur JD, Heald R (2013). Mitotic spindle scaling during Xenopus development by kif2a and importin α. eLife 2, e00290.

Wong Y-H, Lee T-Y, Liang H-K, Huang C-M, Wang T-Y, Yang Y-H, Chu C-H, Huang H-D, Ko M-T, Hwang J-K (2007). KinasePhos 2.0: a web server for identifying protein kinase-specific phosphorylation sites based on sequences and coupling patterns. Nucleic Acids Res 35, W588–W594.

Wordeman L, Mitchison TJ (1995). Identification and partial characterization of mitotic centromere-associated kinesin, a kinesin-related protein that associates with centromeres during mitosis. J Cell Biol 128, 95–104.

Yang G, Cameron LA, Maddox PS, Salmon ED, Danuser G (2008). Regional variation of microtubule flux reveals microtubule organization in the metaphase meiotic spindle. J Cell Biol 182, 631–639.

Yang G, Houghtaling BR, Gaetz J, Liu JZ, Danuser G, Kapoor TM (2007). Architectural dynamics of the meiotic spindle revealed by single-fluorophore imaging. Nat Cell Biol 9, 1233–1242.

Zhang X, Ems-McClung SC, Walczak CE (2008). Aurora A phosphorylates MCAK to control ran-dependent spindle bipolarity. Mol Biol Cell 19, 2752–2765.

Zhang X, Lan W, Ems-McClung SC, Stukenberg PT, Walczak CE (2007). Aurora B phosphorylates multiple sites on mitotic centromere-associated kinesin to spatially and temporally regulate its function. Mol Biol Cell 18, 3264–3276.

Zhang L, Shao H, Huang Y, Yan F, Chu Y, Hou H, Zhu M, Fu C, Aikhionbare F, Fang G, *et al*. (2011). PLK1 phosphorylates mitotic centromere-associated kinesin and promotes its depolymerase activity. J Biol Chem 286, 3033–3046.